

Ghost in the Shell: Evidence for Past AGN Activities in NGC 5195 from a Newly Discovered large-scale Ionized Structure

XIAOYU XU (许啸宇) ¹ AND JUNFENG WANG ¹

¹*Department of Astronomy, Xiamen University, Xiamen, Fujian 361005, China*

ABSTRACT

The early-type galaxy NGC 5195 (alternatively known as M51b) possesses extended gas features detected in multi-wavelength, postulated to be associated with previous activities of the central supermassive black hole (SMBH). Using integral field spectroscopic observations from the Canada-France-Hawaii Telescope (CFHT)/SITELE, we report on the discovery of a new large-scale ionized gas structure traced by [O III], [N II], and H α line emission, extending to ~ 10 kpc from the nucleus of NGC 5195. Its bipolar morphology, emission line ratio diagnostics, and comparison with the X-ray image from *Chandra* and low-frequency radio data from *LOFAR* all indicate that it is likely an outflow inflated by a past episode of elevated active galactic nucleus (AGN) activity. Assuming the ionized gas is outflowing from the central region of NGC 5195, the estimated mass and energy outflow rates are $\dot{M}_{\text{out}} = 3.5\text{--}27.9 M_{\odot} \text{ yr}^{-1}$ and $\dot{E}_{\text{out}} = 0.98\text{--}7.9 \times 10^{40} \text{ erg s}^{-1}$, respectively, which cannot be provided by current star formation and the low luminosity nucleus. Alternatively, considering the history of gravitational interaction between the M51 pair and the presence of HI tidal tail, the northern large-scale ionized gas could very likely be associated with tidally stripped material illuminated by a luminous AGN in the past.

Keywords: Interacting galaxies(802) — LINER galaxies(925) — Interstellar medium(847) — Circumgalactic medium(1879)

1. INTRODUCTION

Galaxy interactions and mergers are thought to play an important role in triggering star formation and active galactic nuclei (AGNs) activities. Galactic outflows driven by AGNs are predicted by theoretical models and simulations during such a key stage of galaxy evolution. Unequivocally, multiphase AGN outflows on various scales have been detected in galaxies at different redshifts (e.g. Fabian 2012; Tombesi et al. 2015; Woo et al. 2016; Venturi et al. 2018). Such AGN activities are postulated to be episodic, possibly governed by accretion disk physics and large-scale gas supply (Shankar et al. 2009; Shen 2021). The impact on the surrounding galactic medium leaves imprints that provide useful diagnostics on the historic radiative and mechanical power of these AGNs (e.g., Schweizer et al. 2013; Sartori et al. 2016; Keel et al. 2017; Harvey et al. 2022).

The interacting system Messier 51 (M51) contains a grand design spiral galaxy NGC 5194 (M51a) and an early-type galaxy NGC 5195 (M51b). NGC 5195 is classified as different types of the galaxy, such as SB0₁-pec (Sandage & Tammann 1981) and I0-pec (de Vaucouleurs et al. 1991), due to its peculiar morphology that is tidally disturbed in the interaction. An SMBH with mass $M_{\text{BH}} \sim 10^7 M_{\odot}$ is believed to reside in the nucleus of NGC 5195 (e.g. Schlegel et al. 2016; Rampadarath et al. 2018). According to the optical emission-line ratios, the nucleus is classified as the low ionization nuclear emission-line region (LINER) (Ho et al. 1997). An AGN is suggested to inhabit the center of this galaxy based on the detection of the high-excitation emission line [Ne v] $\lambda 14.32 \mu\text{m}$ (Goulding & Alexander 2009). The current level of the nuclear activity of NGC 5195 is expected to be very low with an unabsorbed X-ray luminosity of $L_{0.3\text{--}10 \text{ keV}} \sim 1.3 \times 10^{38} \text{ erg s}^{-1}$ and weak radio emission of $L_{8.6 \text{ GHz}} < 8.7 \times 10^{34} \text{ erg s}^{-1}$ (e.g. Rampadarath et al. 2018).

Schlegel et al. (2016) revealed a double-arc-like X-ray structure in the southern region of the NGC 5195 nu-

cleus with $\sim 15''$ – $30''$ away from the center using the *Chandra* data. A slender $H\alpha$ -emitting feature (first detected by Greenawalt et al. 1998) locates just outside the outer X-ray arc, which was expected to be plowed up by the X-ray-emitting gaseous outflow. They attributed the arcs to episodic outbursts of the nuclear SMBH. Later Rampadarath et al. (2018) confirmed the kpc-scale arcs in the radio bands with Very Large Array (VLA) observations and detected a linear radio spur near the nucleus pointing towards the arcs. They suggested that the kpc-scale structures likely resemble a jet-inflated bubble associated with past AGN activities. Additionally, a vast $H\alpha$ cloud $\sim 13'$ north of the M51 system was detected by Watkins et al. (2018), which was expected to be associated with the tidal stripping or AGN activities during the interaction.

In this work, we present the results of our new integral field spectroscopic (IFS) observations focusing on the large ionized gas structure in NGC 5195. The observations and data reduction are described in Section 2. Main results including the flux and velocity maps, the emission-line diagnostic diagram and map, and the comparison with other observational results in different bands are presented in Section 3. In Section 4 and Section 5, we discuss the findings and draw brief conclusions. For consistency with Schlegel et al. (2016) and Rampadarath et al. (2018), the distance to NGC 5195 is adopted as $D = 8.0$ Mpc ($1'' \approx 40$ pc).

2. OBSERVATIONS AND DATA REDUCTION

2.1. CFHT/SITELLE data

NGC 5195 was observed by the instrument SITELLE (Grandmont et al. 2012) installed on the 3.6m CFHT, on 2019-04-08, 2019-04-10, and 2019-05-10 (Program 19AS002, PI: J. Wang). SITELLE is an imaging Fourier transform spectrometer (IFTS) designed for the CFHT, which can provide IFS abilities in the visible band (350 to 900 nm), with a large field of view (FOV) $\sim 11 \times 11$ arcmin² and variable spectral resolution ($R = 2$ to 10000) (Drissen et al. 2019). We used the SN2 (480-520 nm) and SN3 (651-685 nm) filters, with exposure time ~ 4.5 hours for SN2 and ~ 3.55 hours for SN3, to cover main emission lines e.g. $H\alpha$, $H\beta$, [O III] $\lambda\lambda 4959, 5007$, [N II] $\lambda\lambda 6548, 6583$, and [S II] $\lambda\lambda 6716, 6731$. The spectral resolution of the SN2 and SN3 datacubes is set to be $R \sim 1150$.

The calibrated datacubes of SN2 and SN3 were retrieved from the Canadian Astronomy Data Centre

(CADC)¹. The ORCS² (Martin et al. 2015) is used to analyse the data, which is a python module for analysis of SITELLE spectral cubes. To obtain extended emission lines with enough signal-to-noise ratio (SNR), we rebinned the spectral cubes with a factor of 10. The Voronoi binning technique (Cappellari & Copin 2003) was also used to rebin the datacubes for cross-checking the faint extended structure. Comparing the results of these two binning methods, no significant improvements can be gained using the Voronoi binning, hence the 10×10 binning is sufficient for the main purpose of this work. We follow the method described by Rousseau-Nepton et al. (2018) to subtract the stellar continuum from the spectra. The spectrum without emission lines extracted from the nuclear region with a radius of $\sim 5.1'' \times 5.1''$ is used as the continuum template, which is subtracted in every spectrum extracted from the FOV after normalized to the continuum levels of those spectra. Due to the low spectral resolution, we only used the ‘‘sinc’’ model, the natural instrument line shape of IFTS, to fit emission lines of the SN2 and SN3 datacube and thus we cannot obtain the velocity dispersion of emission lines. We followed the procedure described in Martin et al. (2018) to refine the wavelength calibration by measuring the velocity of the night sky emission lines.

For the extinction correction, the flux ratio of $H\alpha$ and $H\beta$ (the Balmer decrement) was used. The attenuation law from Calzetti (2001) and an intrinsic Balmer decrement $H\alpha/H\beta = 3.1$ (Osterbrock & Ferland 2006) were adopted.

Figure 1 shows the deep image derived from the SN2 datacube. The region covering NGC 5195 is selected for fitting and analysis, shown as a white box. A large circle region far away from the M51 system and including no apparent point sources is selected to extract a spectrum as the background. Two examples of spectra extracted from the red circular region in the left panel of Figure 1 are shown in the right panels, in which the top is for the SN2 and the bottom is for the SN3 datacube. The spectral fitting illustrates that the continuum templates perform well especially for the $H\beta$ emission line fitting.

2.2. Chandra X-ray data

The X-ray emission of the NGC 5195 has been thoroughly studied in detail by Schlegel et al. (2016) and Rampadarath et al. (2018). This work would not repeat their analysis but only derive the soft X-ray image to compare with our IFS results. We obtained all

¹ <https://www.cadc-ccda.hia-ihp.nrc-cnrc.gc.ca/en/>

² <https://github.com/thomasorb/orcs>

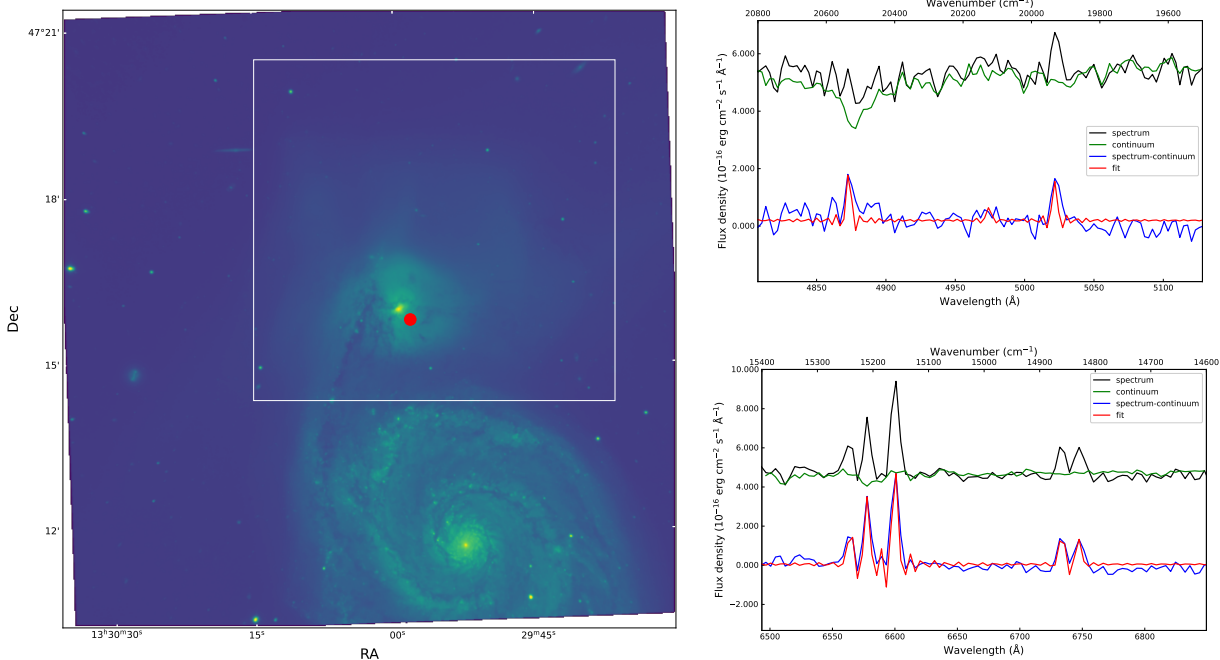


Figure 1. Left: The deep broad-band image of M51 obtained from SITELE’s SN2 datacube. The large spiral galaxy in the south is the NGC 5194 and the NGC 5195 is the smaller one above the NGC 5194. The white box denotes the region for fitting and analysis. North is to the top, and east to the left. Top right: A spectrum (black) with the continuum template (green), emission-line residual (blue), and fitting model (red) extracted from the red circle region in the left panel of the SN2 datacube. Bottom right: Same as the top right but extracted from the SN3 datacube.

available *Chandra* observations of M51 from *Chandra* Data Archive³ except ObsID 414 and ObsID 12562 (for the reason described in Schlegel et al. 2016), including all data used by Schlegel et al. (2016) and Rampadarath et al. (2018) supplemented with ObsID 20998, 23472, 23473, 23474, and 23475. The total exposure time reaches 1.04 Ms. All data were reprocessed and merged using CIAO 4.13 (Fruscione et al. 2006) with CALDB version 4.9.4.

3. RESULTS

3.1. Flux and velocity maps

In Figure 2, the rebinned flux maps of $H\beta$, $[O\ III]\lambda 5007$, $H\alpha$, and $[N\ II]\lambda 6583$ are shown. Due to the low SNRs of $[S\ II]\lambda\lambda 6716, 6731$ in most spaxels, we do not show the flux maps of these two emission lines. To obtain robust measurements, the spaxels with $SNR < 3$ are rejected. Note that the lowest level of flux contours shown corresponds to 2×10^{-17} erg cm^{-2} s^{-1} , and emission structures fainter than this threshold are not reliable, which can be affected by the instrumental mod-

ulation of SITELE. The most intriguing structure is the large hook-like $[O\ III]$ cloud (region A and B in Figure 2(b)) in the north of NGC 5195, extending $\sim 4'$ in projection (~ 10 kpc) from the nucleus, which is not known from previous works. Its presence is further confirmed in the $[N\ II]$ flux map. The $H\alpha$ flux maps also show extended features in the region B along the direction of the $[O\ III]$ hook with $\sim 3'$ away from the nucleus. This ionized gas structure is consistent with a similar faint bubble-like $H\alpha$ feature detected by Watkins et al. (2018) using deep narrow-band imaging. Although the $H\beta$ flux map exhibit relatively weak emission, the main features are basically consistent with other flux maps.

In previous studies, a double arc-like structure in the south region of NGC 5195 had been detected in the soft X-ray band (Schlegel et al. 2016), and corresponding structures are detected in $H\alpha$ narrowband image and 20 cm radio band (Greenawalt et al. 1998; Schlegel et al. 2016; Rampadarath et al. 2018). These structures can also be found in our emission-line flux maps, e.g. a blurred arc feature in $H\alpha$, $[O\ III]$, and $[N\ II]$ map (region D), which is extending to $\sim 70''$ (for $[O\ III]$) in projection.

³ <https://cda.harvard.edu/chaser/>

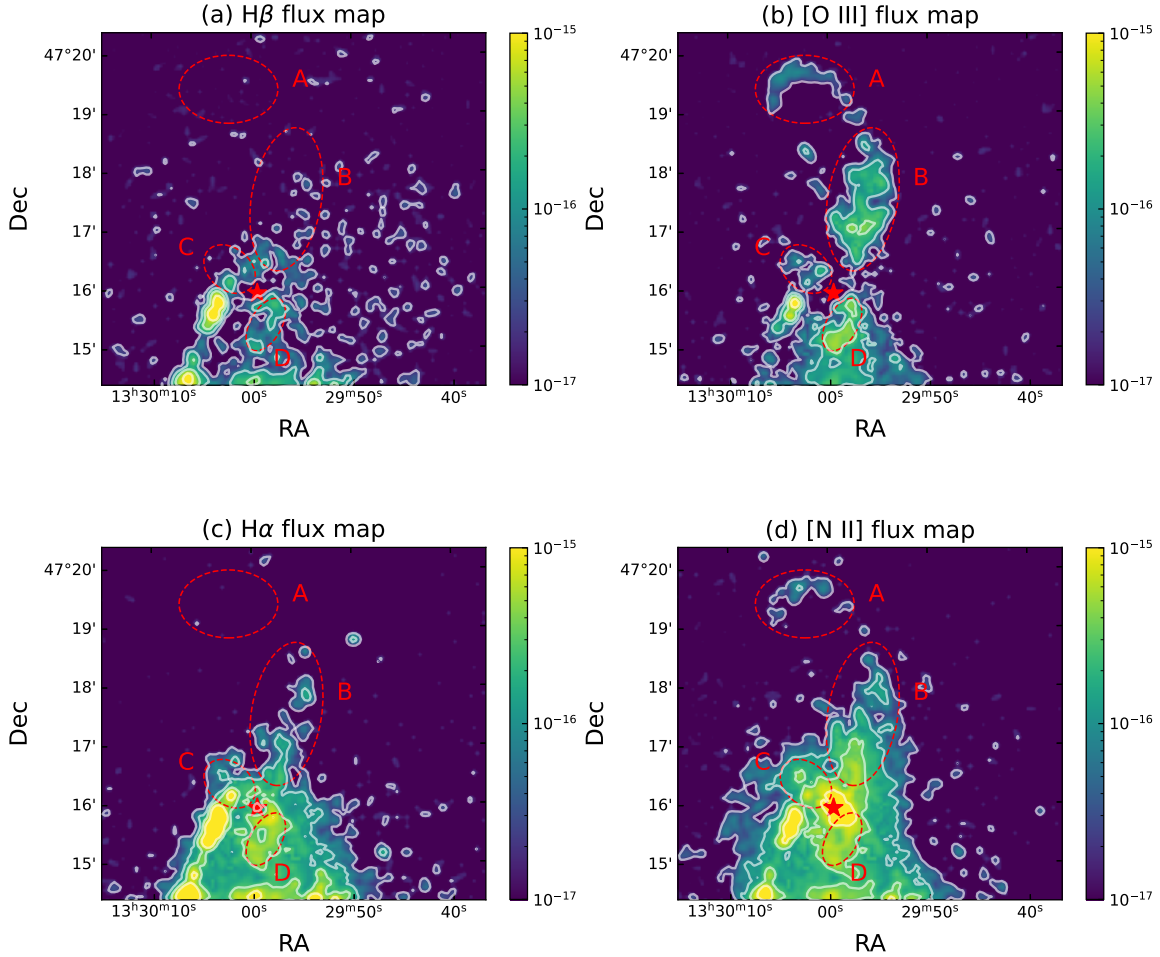


Figure 2. (a): 10×10 binned and smoothed (Gaussian kernel with radius of 1 spaxel) flux map of $H\beta$ emission line superposed with its flux contours. The contour levels are 2×10^{-17} , 1×10^{-16} , 3×10^{-16} , and 9×10^{-16} . The unit of the colorbar is $\text{erg cm}^{-2} \text{s}^{-1}$. The spaxels with $\text{SNR} < 3$ are rejected. (b), (c), and (d) are the same as (a) but for $[\text{O III}]\lambda 5007$, $H\alpha$, and $[\text{N II}]\lambda 6583$, respectively. The red star marks the NGC 5195 nucleus. Four red dashed elliptical regions are labeled as A, B, C, and D, respectively.

$[\text{O III}]$ emission appears to be very weak or absent in the nuclear region. The dust extinction in the nuclear region of NGC 5195 is up to $A_V = 1.67$ mag (Wei et al. 2021), which can reduce the observed flux of the $[\text{O III}]$ emission line. Considering the low X-ray (an absorption corrected luminosity $L_{0.3-10 \text{ keV}} \sim 1.3 \times 10^{38} \text{ erg s}^{-1}$) and radio luminosity ($L_{8.6 \text{ GHz}} < 8.7 \times 10^{34} \text{ erg s}^{-1}$) in the nuclear region of NGC 5195 (e.g. Rampadarath et al. 2018), the nuclear $[\text{O III}]$ emission is considered to be intrinsically very weak.

In all these flux maps, a spiral arm from the NGC 5194 connecting with region C can be seen in the southeastern region of the NGC 5195’s nucleus. A low flux gap can be seen in the bottom of the FoV and under region D in all flux maps, which is suggestive that the gap separates the ionized gas emission from NGC 5195 (above the gap) and NGC 5194 (under the gap).

In Figure 3, the velocity maps of $[\text{O III}]$, $H\alpha$, and $[\text{N II}]$ are presented. The systemic velocity 571 km s^{-1} of NGC 5195 (Falco et al. 1999) is used to calibrate these velocity maps. As the $[\text{O III}]$ velocity map shows, the velocities in regions A, B, and C are redshifted while in region D are blueshifted, which is suggestive of a bipolar outflow. Other velocity maps also support this interpretation. Considering the strong interaction between NGC 5195 and NGC 5194, the northern ionized gas structure can also be produced by tidal stripping. The highest velocity gas is seen in region A with the median velocity of $[\text{O III}]$ emission line reaching $\sim 270 \text{ km s}^{-1}$. The median velocities of $[\text{O III}]$ in the region B, C and D are $\sim 170 \text{ km s}^{-1}$, $\sim 100 \text{ km s}^{-1}$ and $\sim -50 \text{ km s}^{-1}$, respectively. The $[\text{N II}]$ and $H\alpha$ velocity maps also exhibit similar kinematics as the $[\text{O III}]$ map in these four regions.

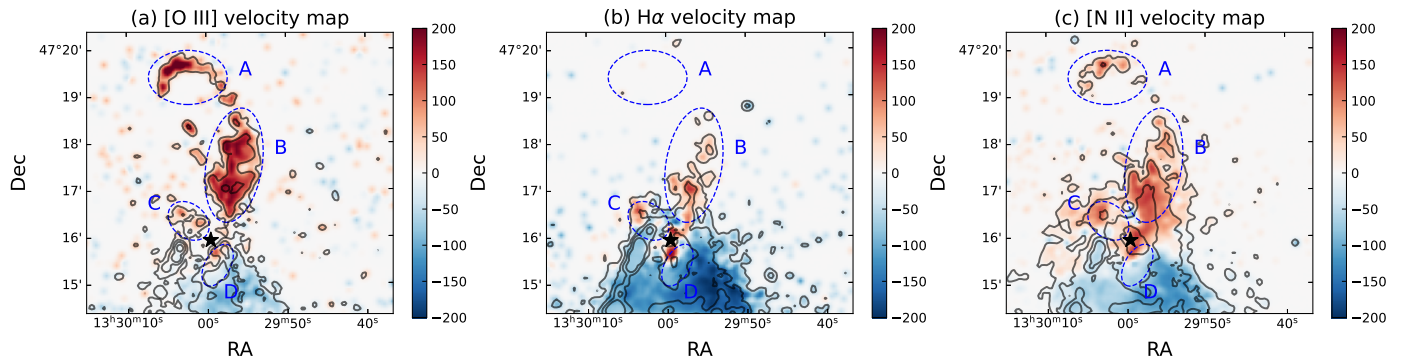


Figure 3. (a): 10×10 binned and smoothed (Gaussian kernel with a radius of 1 spaxel) velocity map of $[\text{O III}]\lambda 5007$ superposed with the flux contours (same as contours in Figure 2). (b) and (c) are the same as (a) but for $\text{H}\alpha$ and $[\text{N II}]\lambda 6583$, respectively. The black star marks the position of the NGC 5195 nucleus and the four dashed regions are the same as those in Figure 2.

3.2. Emission-line diagnostic diagram and map

The Baldwin, Phillips, and Telervich (BPT) diagnostic diagram (Baldwin et al. 1981) is usually used to distinguish the ionization and excitation mechanisms of the ionized gas. To obtain statistically robust results, the spaxels with the flux of the $[\text{O III}]\lambda 5007$ ($F_{[\text{O III}]}$) or the $[\text{N II}]\lambda 6583$ ($F_{[\text{N II}]}$) lower than $2 \times 10^{-17} \text{ erg cm}^{-2} \text{ s}^{-1}$ are masked out in the diagram and map. For spaxels with the flux of $\text{H}\alpha$ of $F_{\text{H}\alpha} < 10^{-17} \text{ erg cm}^{-2} \text{ s}^{-1}$, upper limits of Balmer emission lines of $F_{\text{H}\alpha} = 10^{-17} \text{ erg cm}^{-2} \text{ s}^{-1}$ and $F_{\text{H}\beta} = F_{\text{H}\alpha}/3.1$ are given.

In Figure 4, the BPT diagram and map are presented. The ionization sources in NGC 5195 are dominated by AGN and LINER. Region A and B are dominated by AGN photoionization, only the edges of region B are classified as LINER. In region D, the LINER dominates the area near the nucleus, while the AGN becomes the main source of ionization with the increasing distance to the nucleus.

The spiral arm under region C, which is from NGC 5194, is dominated by regions classified as HII and composite. Considering the bottom of the field is dominated by composite regions and the lower part of the FoV is located at a spiral arm of NGC 5194 (Figure 1), most of the ionized gas here should be from the NGC 5194, which is consistent with our initial suggestion in Section 3.1.

3.3. Comparison with the radio and X-ray data

Figure 5(a) and (b) show the adaptively smoothed *Chandra* soft X-ray (0.4–2.0 keV) image superposed with contours of $[\text{O III}]\lambda 5007$ and $\text{H}\alpha$ emission, respectively. The southern double-arc-like X-ray structure found by Schlegel et al. (2016) is spatially coincident with the in-

ner part of $[\text{O III}]\lambda 5007$ arc (region D), whereas the northern extended X-ray feature is inside the rims of the northern $[\text{O III}]\lambda 5007$ structure (region B and C). Compared to the $\text{H}\alpha$ flux contours, the soft X-ray emission also corresponds to the diffuse $\text{H}\alpha$ structure spatially, which is consistent with previous works (Schlegel et al. 2016; Rampadarath et al. 2018).

The Low Frequency Array (LOFAR) 151 MHz images (Mulcahy et al. 2014) superposed with contours of $[\text{O III}]\lambda 5007$ and $\text{H}\alpha$ are presented in Figure 5(c) and (d), respectively. As Figure 5(c) shows, a radio lobe or bubble extends from the nucleus to the northeast and just inside the northern $[\text{O III}]\lambda 5007$ emission, indicating a likely association with a jet or outflow. In Figure 5(d), the northern $\text{H}\alpha$ structure is similar to $[\text{O III}]\lambda 5007$ but extends to a smaller scale. The low-frequency radio extension is consistent with the northern radio bubble detected by Rampadarath et al. (2018) using VLA, although that bubble-like feature is weaker with a smaller scale. Note that Rampadarath et al. (2018) also detected a radio bubble in L, C, and X bands in the southern region, which is spatially associated with the southern $\text{H}\alpha$, $[\text{O III}]\lambda 5007$, and soft X-ray emission features.

4. DISCUSSION

4.1. Origin of the large-scale ionized gas structure

As the flux and velocity maps show (Figure 2 and 3), the main ionized gas structure in NGC 5195 (regions A, B, C, and D) closely resembles a bipolar outflow. According to the bubble-like morphology detected in different bands ($[\text{O III}]\lambda 5007$, $\text{H}\alpha$, $[\text{N II}]\lambda 6583$, and the soft X-ray) and the corresponding LOFAR radio bubble feature (Figure 5), we suggest that this large-scale ionized structure can be associated with an AGN jet or outflow, which

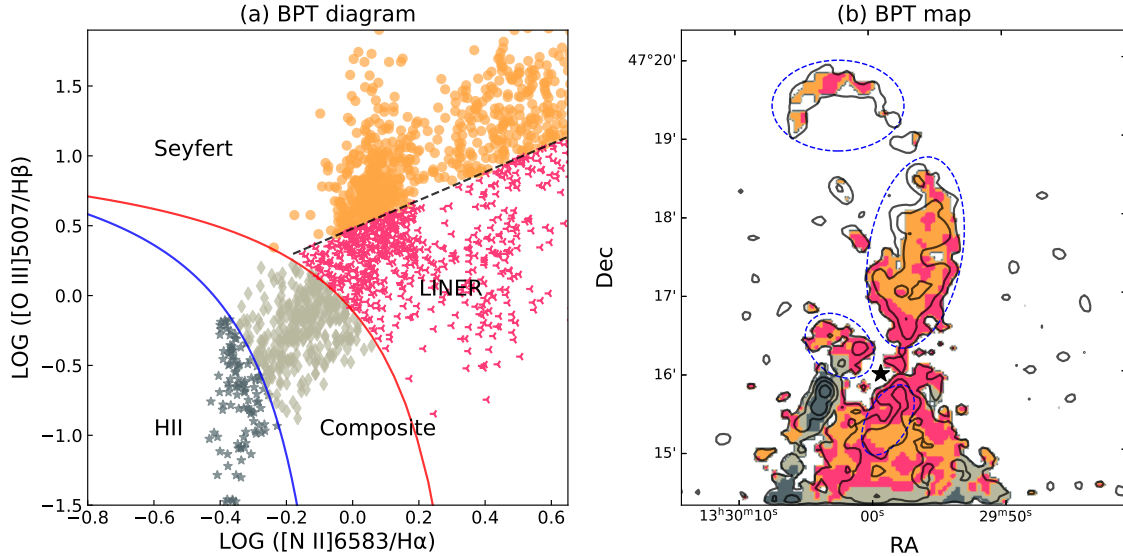


Figure 4. (a): The BPT diagnostic diagram. The blue solid line is the classification boundary in [Kauffmann et al. \(2003\)](#) for finding AGN. The red solid line shows the theoretical upper limit for star-forming galaxies ([Kewley et al. 2001](#)), which separates the composite emission and AGN/LINER. The dashed line ([Cid Fernandes et al. 2010](#)) shows the division between AGN and LINER. (b): Spatially resolved BPT map. The colors denote different ionization mechanisms in (a).

is consistent with [Rampadarath et al. \(2018\)](#) but on a larger scale. The BPT diagram and map (Figure 4) also suggest that the main ionized structures (regions A, B, and D) should be photoionized by an AGN. The LINER regions in the BPT map spatially correspond to the superposed areas of the soft X-ray, radio, and ionized gas emission, which indicates these regions can be excited by the shocks produced by a jet or outflow. Considering the current low state of the SMBH in the center of NGC 5195 ([Rampadarath et al. 2018](#)) and the weak [O III] flux in the nuclear region, the large-scale ionized gas structure should relate to past epochs of AGN activities, which is consistent with the suggestion in previous works ([Schlegel et al. 2016](#); [Rampadarath et al. 2018](#)).

The dynamical timescale of the ionized outflow can be estimated to be $t_{\text{dyn}} \approx D_{\text{out}}/v_{\text{out}} = 30$ Myr, where $D_{\text{out}} \sim 10$ kpc denotes the distance away from the nucleus and $v_{\text{out}} \sim 300$ km s⁻¹ is the outflow velocity. The simulation expects that the recent interaction between NGC 5195 and NGC 5194 has occurred ≈ 50 –100 Myr ago ([Salo & Laurikainen 2000](#)). Considering the gas infalling timescale ([Schlegel et al. 2016](#)), the dynamical timescale of the ionized outflow is roughly corresponding to the recent interaction between NGC 5195 and NGC 5194.

Distant ionized clouds originated from tidal stripping and illuminated by past AGN activities have been detected in some galaxies (e.g. [Keel et al. 2017](#)), and such a connection appears to be quite common as revealed

by systematic surveys ([Keel et al. 2022](#)). The Hanny’s Voorwerp is a famous example extending ~ 50 kpc in projection from the nucleus of IC 2497, which is inferred as a part of massive HI tidal tail and photoionized by past luminous AGN ([Józsa et al. 2009](#); [Lintott et al. 2009](#); [Keel et al. 2012](#)). In the M51 system, large-scale neutral gas structures originating from tidal stripping have been revealed by [Rots et al. \(1990\)](#) using VLA. The large ionized gas structure (regions A and B) is coincident with a part of a giant tidal tail traced by HI emission extending from NGC 5195 to the north. Considering the velocity of the corresponding HI tidal feature is about 30–90 km s⁻¹ ([Rots et al. 1990](#)), which is several times lower than the median velocity (~ 170 –270 km s⁻¹) of the northern [O III] structure, the ionized gas feature may be a shocked, relatively higher velocity component of the tidal stream or photoionized and accelerated by a more active AGN in the past. Combining the dominant AGN photoionization mechanism in this ionized structure suggested by the BPT diagram, the spatial correspondence with the HI tidal tail and the faded AGN in the nucleus of NGC 5195, the northern large-scale ionized gas structure is similar to Hanny’s Voorwerp, which can be a part of tidal tail photoionized by past AGN activities.

In fact, tidal stripping and AGN activities can both be important here. In such complicated interacting galaxy pairs, it is challenging to pinpoint the origin of the large-

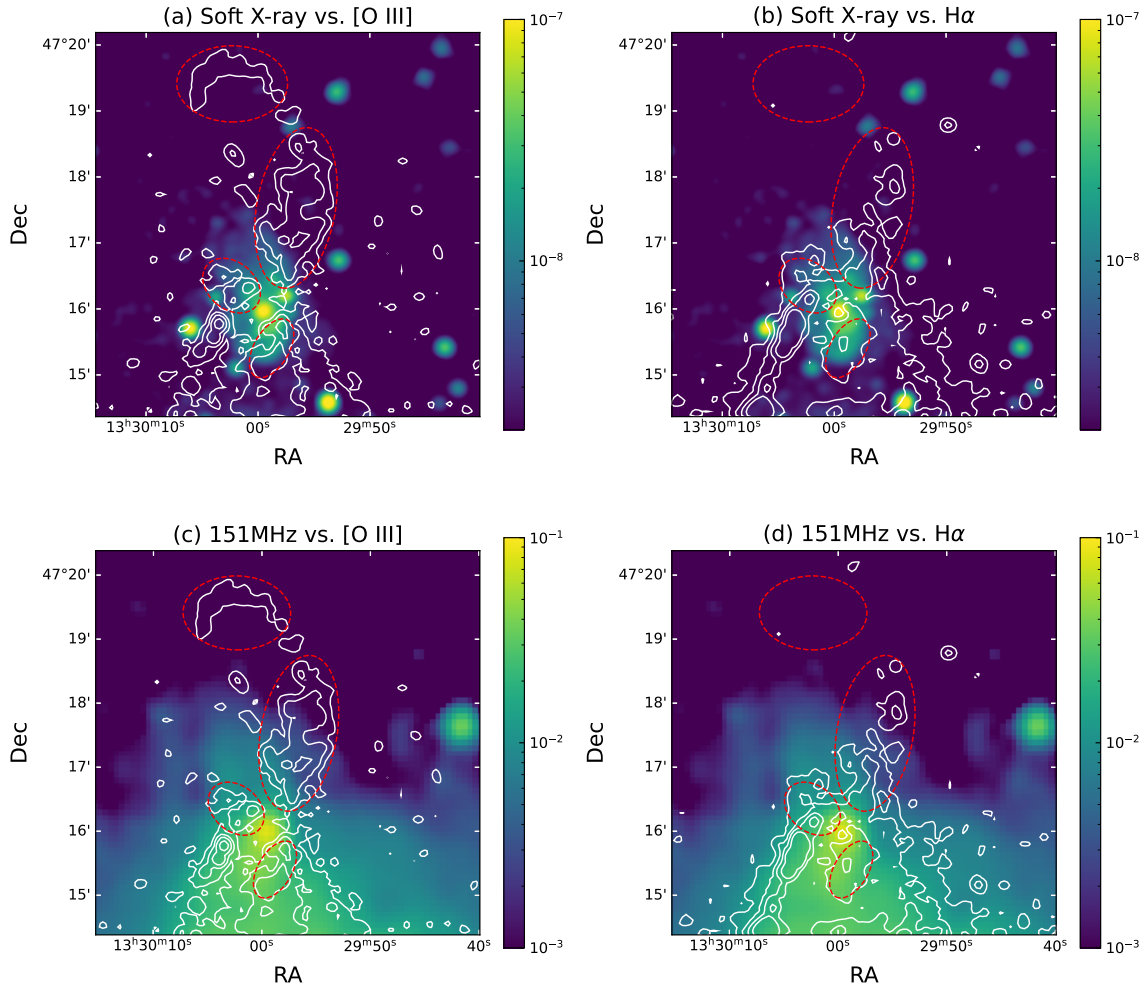


Figure 5. (a): *Chandra* soft X-ray (0.4–2.0 keV) image superposed with the contours of [O III]λ5007 flux. The unit of the colorbar is $\text{counts cm}^{-2} \text{s}^{-1}$. (b): Same as (a) but superposed with the contours of H α emission. (c): LOFAR 151 MHz image (Mulcahy et al. 2014) superposed with the contours of [O III]λ5007 flux. The unit of the colorbar is Jy/beam. (d): Same as (c) but superposed with the contours of H α emission. The red dashed elliptical regions are the same as those in Figure 2.

scale ionized gas structure. More sensitive observations on the faint structures are needed to resolve this issue.

4.2. Energetics of the ionized outflow

Assuming the ionized gas structure in NGC 5195 is a biconical outflow, we can estimate the mass and energy outflow rate. The mass of an ionized outflow can be estimated using H β emission line (e.g. Harrison et al. 2014) or [O III]λ5007 line (e.g. Carniani et al. 2015; Karouzos et al. 2016). We firstly use the [O III]λ5007 line to calculate the outflow mass following (e.g. Carniani et al. 2015):

$$M_{\text{gas}} = 4 \times 10^8 \left(\frac{L_{[\text{OIII}]}}{10^{44} \text{ erg s}^{-1}} \right) \left(\frac{100 \text{ cm}^{-3}}{n_e} \right) M_{\odot}, \quad (1)$$

where $L_{[\text{OIII}]}$ is the luminosity of [O III]λ5007 and n_e is the electron density, assuming the solar metallicity. The

electron density can be estimated from the flux ratio of [S II]λ6716/[S II]λ6731, assuming the case B and the electron temperature $T_e = 10^4$ K (Osterbrock & Ferland 2006). However, the [S II] doublets are very weak in most areas of our datacube, especially in regions A, B, and C. In region D, the [S II] doublets can be fitted but with $\text{SNR} < 3$, and the corresponding n_e is estimated to be a very low value ($< 1 \text{ cm}^{-3}$), which is much lower than the sensitive range ($10 < n_e < 10^4 \text{ cm}^{-3}$) of these doublets (Osterbrock & Ferland 2006). Rampadarath et al. (2018) estimated the density to be $n_e \approx 0.01 \text{ cm}^{-3}$ following the method described by Pakull et al. (2006), which is consistent with the very low value indicated by the flux ratio of the [S II] doublets. The mass and energy

outflow rate can be calculated following:

$$\dot{M}_{\text{out}} = 3M_{\text{gas}} \frac{v_{\text{out}}}{R_{\text{out}}}, \quad (2)$$

$$\dot{E}_{\text{out}} = \frac{1}{2} \dot{M}_{\text{out}} v_{\text{out}}^2, \quad (3)$$

where v_{out} denotes the averaged velocity of the outflow, and R_{out} is the outflow size. Only the luminosity of [O III] from regions A, B, C, and D is considered in estimating the outflow rates. Adopting $n_e = 0.01 \text{ cm}^{-3}$, $R_{\text{out}} = 10 \text{ kpc}$, and $v_{\text{out}} = 300 \text{ km s}^{-1}$, we obtain $\dot{M}_{\text{out}} = 3.5 M_{\odot} \text{ yr}^{-1}$ and $\dot{E}_{\text{out}} = 9.8 \times 10^{40} \text{ erg s}^{-1}$. This estimated \dot{E}_{out} is lower than but consistent with the value (a few $10^{41} \text{ erg s}^{-1}$) calculated by Rampadarath et al. (2018), because the outflow mass estimated from the [O III] λ 5007 flux is normally a lower limit (Carniani et al. 2015).

The upper limit of outflow mass can be estimated using the total $H\beta$ luminosity of NGC 5195, which is derived using $L_{H\beta} \sim L_{H\alpha}/3.1 = 4.5 \times 10^{38} \text{ erg s}^{-1}$. The outflow mass traced by $H\beta$ emission line can be calculated following (e.g. Harrison et al. 2014; Xu & Wang 2022):

$$M_{\text{gas}} = 6.78 \times 10^8 \left(\frac{L_{H\beta}}{10^{43} \text{ erg s}^{-1}} \right) \left(\frac{100 \text{ cm}^{-3}}{n_e} \right) M_{\odot}. \quad (4)$$

We obtain the upper limits of the mass and energy outflow rate of $\dot{M}_{\text{out,max}} = 27.9 M_{\odot} \text{ yr}^{-1}$ and $\dot{E}_{\text{out,max}} = 7.9 \times 10^{41} \text{ erg s}^{-1}$, respectively, which are nearly one order of magnitude larger than the lower limits.

Comparing with the kinetic power resulting from the stellar winds and SNe (Rampadarath et al. 2018) given the current SFR $\approx 0.1 M_{\odot} \text{ yr}^{-1}$ of NGC 5195 (Alatalo et al. 2016), even the lower limit of the energy outflow rate is larger by a factor of two to three, which imply that the current star formation process cannot drive the ionized outflow. A starburst that occurred 370–480 Myr ago had been suggested by Mentuch Cooper et al. (2012), while this is not consistent with the timescale of the ionized outflow ($t_{\text{dyn}} \approx 30 \text{ Myr}$).

To compare the outflow rates of NGC 5195 with observational results of other AGNs, we show the outflow rates as a function of the AGN bolometric luminosity following Fiore et al. (2017) in the Figure 6. The green regions in the two panels denote the ranges of the outflow rates derived above. The outflow rates of NGC 5195 are comparable to the lower part of the correlations. If the ionized outflow of NGC 5195 is radiatively driven by the AGN and follows the correlation of Fiore et al. (2017), an AGN bolometric luminosity of $L_{\text{bol}} \sim 10^{44.4} - 10^{45.9} \text{ erg s}^{-1}$ is inferred, which is approaching or exceed the Eddington luminosity of $L_{\text{Edd}} \sim 1.3 \times 10^{45} \text{ erg s}^{-1}$,

adopting $M_{\text{BH}} \sim 10^7 M_{\odot}$ for the mass of the SMBH. Alternatively, if the ionized outflow is driven by an AGN jet (Rampadarath et al. 2018), the outflow rate can be much higher than expected from the correlation of Fiore et al. (2017) for a low luminosity AGN. In either case, the outflow is likely powered by the past powerful AGN activities, given that the AGN in NGC 5195 is currently very weak with a small-scale radio jet (e.g. Schlegel et al. 2016; Rampadarath et al. 2018).

Combining the large size and the relatively high outflow rates of this bipolar outflow, feedback effects might be significant in this galaxy.

5. CONCLUSIONS

In this work, we report the observation of the nearby interacting galaxy NGC 5195 using the CFHT/SITELLE, and study the spatially resolved ionized gas. To identify the ionization mechanism of the emission line gas structure, the BPT diagnostic diagram and map are derived. Multiwavelength observations including the soft X-ray (0.4–2.0 keV) data from the *Chandra* archive and the LOFAR 151 MHz image from Mulcahy et al. (2014) are used to compare with our spatially resolved data. The main results and conclusions are summarized as follows:

1. A remarkable $\sim 10 \text{ kpc}$ scale (in projection) ionized structure traced by [O III], [N II], and $H\alpha$ (less extended) emission lines is discovered (Figure 2 and Figure 3).
2. According to the BPT diagram and map, the large-scale structure is dominated by the region classified as Seyfert and LINER (Figure 4), which indicates that the structure is likely associated with AGN activities or shocks.
3. The northern soft X-ray and the LOFAR 151 MHz bubble-like feature is just located inside the ionized gas structure, which strongly indicates that the ionized gas feature is associated with an AGN jet or outflow (Figure 5). Considering the strong interaction in the M51 system, the northern large-scale ionized gas structure may have a complicated origin. This structure can be a part of the giant HI tidal tail revealed by previous works (Rots et al. 1990) and photoionized by past AGN activities.
4. Assuming the ionized gas structure is a bipolar outflow, the mass and energy outflow rates can be estimated to be $\dot{M}_{\text{out}} = 3.5 - 27.9 M_{\odot} \text{ yr}^{-1}$ and $\dot{E}_{\text{out}} = 0.98 - 7.9 \times 10^{41} \text{ erg s}^{-1}$, which cannot be provided by the current star formation activities (Section 4.2). In lieu of the currently weak AGN,

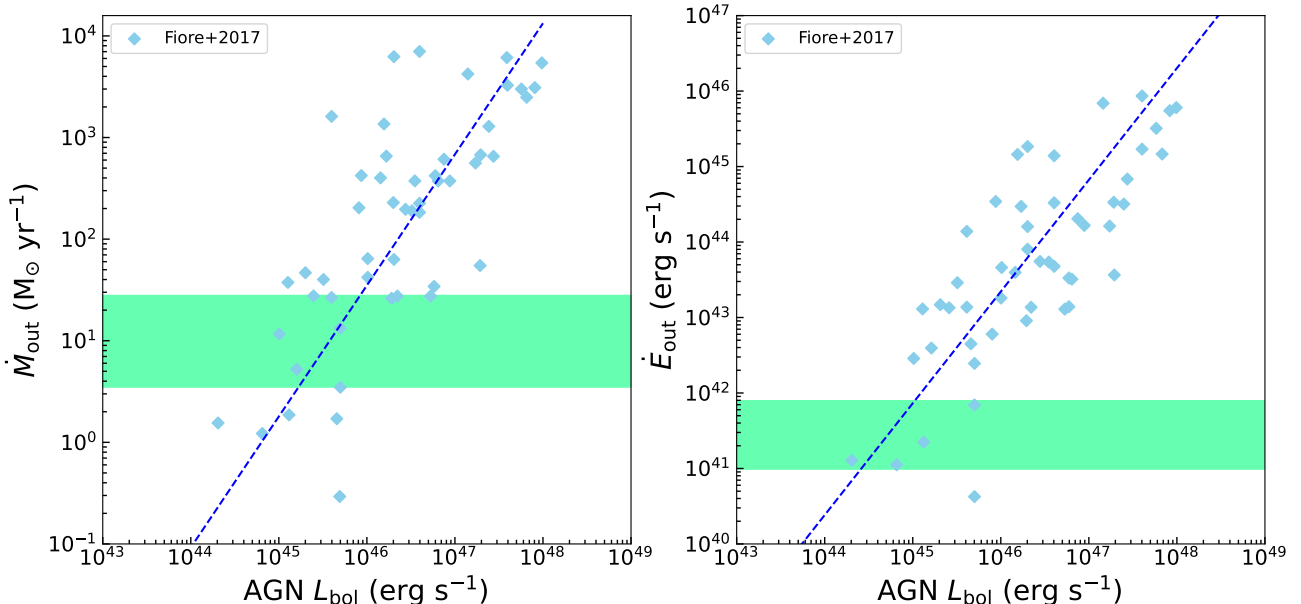


Figure 6. Mass (left panel) and energy (right panel) outflow rate as a function of the AGN bolometric luminosity. The lightblue diamonds denote the ionized outflow measurements from [Fiore et al. \(2017\)](#) and the blue dashed line is their best-fit correlation. The green regions show lower and upper limits of the outflow rates of NGC 5195.

the ionized outflow is likely associated with the past powerful AGN activities.

The NGC 5195 galaxy could be the closest example exhibiting a projected ~ 10 kpc scale ionized structure associated with past AGN outflow/jet activities or light echoes, which makes it an ideal laboratory for studying the AGN feedback, past AGN activities, and the interaction between the galaxy pair. Our future work will study the M51 system in more detail deploying the rich archival multi-wavelength data.

6. ACKNOWLEDGMENTS

We thank the anonymous referee for helpful comments that significantly improved the clarity of our work. We thank Thomas Martin for the instructions on the SITELLE data analysis. J.W. acknowledges the NSFC grants U1831205, 12033004, 12221003 and the science research grants from CMS-CSST-2021-A06 and CMS-CSST-2021-B02. Our SITELLE observation (19AS002) is kindly supported by China Telescope Access Program (TAP). Based on observations obtained at the Canada-France-Hawaii Telescope (CFHT) which is operated from the summit of Maunakea by the Na-

tional Research Council of Canada, the Institut National des Sciences de l’Univers of the Centre National de la Recherche Scientifique of France, and the University of Hawaii. The observations at the Canada-France-Hawaii Telescope were performed with care and respect from the summit of Maunakea which is a significant cultural and historic site. Based on observations obtained with SITELLE, a joint project between Université Laval, ABB-Bomem, Université de Montréal and the CFHT with funding support from the Canada Foundation for Innovation (CFI), the National Sciences and Engineering Research Council of Canada (NSERC), Fond de Recherche du Québec - Nature et Technologies (FRQNT) and CFHT. This research has made use of data obtained from the Chandra Data Archive and the Chandra Source Catalog, and software provided by the Chandra X-ray Center (CXC) in the application packages CIAO and Sherpa.

Facilities: CFHT (SITELLE), CXO (ACIS), LOFAR

Software: astropy ([Astropy Collaboration et al. 2013, 2018](#)), CIAO ([Fruscione et al. 2006](#)), DS9 ([Joye & Mandel 2003](#)), ORCS ([Martin et al. 2015](#))

REFERENCES

Alatalo, K., Aladro, R., Nyland, K., et al. 2016, *The Astrophysical Journal*, 830, 137, doi: [10.3847/0004-637X/830/2/137](https://doi.org/10.3847/0004-637X/830/2/137)

Astropy Collaboration, Robitaille, T. P., Tollerud, E. J., et al. 2013, *Astronomy and Astrophysics*, 558, A33, doi: [10.1051/0004-6361/201322068](https://doi.org/10.1051/0004-6361/201322068)

- Astropy Collaboration, Price-Whelan, A. M., Sipőcz, B. M., et al. 2018, *The Astronomical Journal*, 156, 123, doi: [10.3847/1538-3881/aabc4f](https://doi.org/10.3847/1538-3881/aabc4f)
- Baldwin, J. A., Phillips, M. M., & Terlevich, R. 1981, *Publications of the Astronomical Society of the Pacific*, 93, 5, doi: [10.1086/130766](https://doi.org/10.1086/130766)
- Calzetti, D. 2001, *Publications of the Astronomical Society of the Pacific*, 113, 1449, doi: [10.1086/324269](https://doi.org/10.1086/324269)
- Cappellari, M., & Copin, Y. 2003, *Monthly Notices of the Royal Astronomical Society*, 342, 345, doi: [10.1046/j.1365-8711.2003.06541.x](https://doi.org/10.1046/j.1365-8711.2003.06541.x)
- Carniani, S., Marconi, A., Maiolino, R., et al. 2015, *Astronomy and Astrophysics*, 580, A102, doi: [10.1051/0004-6361/201526557](https://doi.org/10.1051/0004-6361/201526557)
- Cid Fernandes, R., Stasińska, G., Schlickmann, M. S., et al. 2010, *Monthly Notices of the Royal Astronomical Society*, 403, 1036, doi: [10.1111/j.1365-2966.2009.16185.x](https://doi.org/10.1111/j.1365-2966.2009.16185.x)
- de Vaucouleurs, G., de Vaucouleurs, A., Corwin, Herold G., J., et al. 1991, *Third Reference Catalogue of Bright Galaxies*
- Drissen, L., Martin, T., Rousseau-Nepton, L., et al. 2019, *Monthly Notices of the Royal Astronomical Society*, 485, 3930, doi: [10.1093/mnras/stz627](https://doi.org/10.1093/mnras/stz627)
- Fabian, A. C. 2012, *Annual Review of Astronomy and Astrophysics*, 50, 455, doi: [10.1146/annurev-astro-081811-125521](https://doi.org/10.1146/annurev-astro-081811-125521)
- Falco, E. E., Kurtz, M. J., Geller, M. J., et al. 1999, *Publications of the Astronomical Society of the Pacific*, 111, 438, doi: [10.1086/316343](https://doi.org/10.1086/316343)
- Fiore, F., Feruglio, C., Shankar, F., et al. 2017, *Astronomy and Astrophysics*, 601, A143, doi: [10.1051/0004-6361/201629478](https://doi.org/10.1051/0004-6361/201629478)
- Fruscione, A., McDowell, J. C., Allen, G. E., et al. 2006, in *Society of Photo-Optical Instrumentation Engineers (SPIE) Conference Series*, Vol. 6270, *Society of Photo-Optical Instrumentation Engineers (SPIE) Conference Series*, ed. D. R. Silva & R. E. Doxsey, 62701V, doi: [10.1117/12.671760](https://doi.org/10.1117/12.671760)
- Goulding, A. D., & Alexander, D. M. 2009, *Monthly Notices of the Royal Astronomical Society*, 398, 1165, doi: [10.1111/j.1365-2966.2009.15194.x](https://doi.org/10.1111/j.1365-2966.2009.15194.x)
- Grandmont, F., Drissen, L., Mandar, J., Thibault, S., & Baril, M. 2012, in *Society of Photo-Optical Instrumentation Engineers (SPIE) Conference Series*, Vol. 8446, *Ground-based and Airborne Instrumentation for Astronomy IV*, ed. I. S. McLean, S. K. Ramsay, & H. Takami, 84460U, doi: [10.1117/12.926782](https://doi.org/10.1117/12.926782)
- Greenawalt, B., Walterbos, R. A. M., Thilker, D., & Hoopes, C. G. 1998, *The Astrophysical Journal*, 506, 135, doi: [10.1086/306232](https://doi.org/10.1086/306232)
- Harrison, C. M., Alexander, D. M., Mullaney, J. R., & Swinbank, A. M. 2014, *Monthly Notices of the Royal Astronomical Society*, 441, 3306, doi: [10.1093/mnras/stu515](https://doi.org/10.1093/mnras/stu515)
- Harvey, T., Maksym, W. P., Keel, W., et al. 2022, arXiv e-prints, arXiv:2208.05915. <https://arxiv.org/abs/2208.05915>
- Ho, L. C., Filippenko, A. V., & Sargent, W. L. W. 1997, *The Astrophysical Journal Supplement Series*, 112, 315, doi: [10.1086/313041](https://doi.org/10.1086/313041)
- Joye, W. A., & Mandel, E. 2003, in *Astronomical Society of the Pacific Conference Series*, Vol. 295, *Astronomical Data Analysis Software and Systems XII*, ed. H. E. Payne, R. I. Jedrzejewski, & R. N. Hook, 489
- Józsa, G. I. G., Garrett, M. A., Oosterloo, T. A., et al. 2009, *Astronomy and Astrophysics*, 500, L33, doi: [10.1051/0004-6361/200912402](https://doi.org/10.1051/0004-6361/200912402)
- Karouzos, M., Woo, J.-H., & Bae, H.-J. 2016, *The Astrophysical Journal*, 833, 171, doi: [10.3847/1538-4357/833/2/171](https://doi.org/10.3847/1538-4357/833/2/171)
- Kauffmann, G., Heckman, T. M., Tremonti, C., et al. 2003, *Monthly Notices of the Royal Astronomical Society*, 346, 1055, doi: [10.1111/j.1365-2966.2003.07154.x](https://doi.org/10.1111/j.1365-2966.2003.07154.x)
- Keel, W. C., Moiseev, A., Kozlova, D. V., et al. 2022, *Monthly Notices of the Royal Astronomical Society*, 510, 4608, doi: [10.1093/mnras/stab3656](https://doi.org/10.1093/mnras/stab3656)
- Keel, W. C., Lintott, C. J., Schawinski, K., et al. 2012, *The Astronomical Journal*, 144, 66, doi: [10.1088/0004-6256/144/2/66](https://doi.org/10.1088/0004-6256/144/2/66)
- Keel, W. C., Lintott, C. J., Maksym, W. P., et al. 2017, *The Astrophysical Journal*, 835, 256, doi: [10.3847/1538-4357/835/2/256](https://doi.org/10.3847/1538-4357/835/2/256)
- Kewley, L. J., Dopita, M. A., Sutherland, R. S., Heisler, C. A., & Trevena, J. 2001, *The Astrophysical Journal*, 556, 121, doi: [10.1086/321545](https://doi.org/10.1086/321545)
- Lintott, C. J., Schawinski, K., Keel, W., et al. 2009, *Monthly Notices of the Royal Astronomical Society*, 399, 129, doi: [10.1111/j.1365-2966.2009.15299.x](https://doi.org/10.1111/j.1365-2966.2009.15299.x)
- Martin, T., Drissen, L., & Joncas, G. 2015, in *Astronomical Society of the Pacific Conference Series*, Vol. 495, *Astronomical Data Analysis Software and Systems XXIV (ADASS XXIV)*, ed. A. R. Taylor & E. Rosolowsky, 327
- Martin, T. B., Drissen, L., & Melchior, A.-L. 2018, *Monthly Notices of the Royal Astronomical Society*, 473, 4130, doi: [10.1093/mnras/stx2513](https://doi.org/10.1093/mnras/stx2513)
- Mentuch Cooper, E., Wilson, C. D., Foyle, K., et al. 2012, *The Astrophysical Journal*, 755, 165, doi: [10.1088/0004-637X/755/2/165](https://doi.org/10.1088/0004-637X/755/2/165)

- Mulcahy, D. D., Horneffer, A., Beck, R., et al. 2014, *Astronomy and Astrophysics*, 568, A74, doi: [10.1051/0004-6361/201424187](https://doi.org/10.1051/0004-6361/201424187)
- Osterbrock, D. E., & Ferland, G. J. 2006, *Astrophysics of gaseous nebulae and active galactic nuclei*
- Pakull, M. W., Grisé, F., & Motch, C. 2006, in *Populations of High Energy Sources in Galaxies*, ed. E. J. A. Meurs & G. Fabbiano, Vol. 230, 293–297, doi: [10.1017/S1743921306008489](https://doi.org/10.1017/S1743921306008489)
- Rampadarath, H., Soria, R., Urquhart, R., et al. 2018, *Monthly Notices of the Royal Astronomical Society*, 476, 2876, doi: [10.1093/mnras/sty390](https://doi.org/10.1093/mnras/sty390)
- Rots, A. H., Bosma, A., van der Hulst, J. M., Athanassoula, E., & Crane, P. C. 1990, *The Astronomical Journal*, 100, 387, doi: [10.1086/115522](https://doi.org/10.1086/115522)
- Rousseau-Nepton, L., Robert, C., Martin, R. P., Drissen, L., & Martin, T. 2018, *Monthly Notices of the Royal Astronomical Society*, 477, 4152, doi: [10.1093/mnras/sty477](https://doi.org/10.1093/mnras/sty477)
- Salo, H., & Laurikainen, E. 2000, *Monthly Notices of the Royal Astronomical Society*, 319, 377, doi: [10.1046/j.1365-8711.2000.03650.x](https://doi.org/10.1046/j.1365-8711.2000.03650.x)
- Sandage, A., & Tammann, G. A. 1981, *A Revised Shapley-Ames Catalog of Bright Galaxies*
- Sartori, L. F., Schawinski, K., Koss, M., et al. 2016, *MNRAS*, 457, 3629, doi: [10.1093/mnras/stw230](https://doi.org/10.1093/mnras/stw230)
- Schlegel, E. M., Jones, C., Machacek, M., & Vega, L. D. 2016, *The Astrophysical Journal*, 823, 75, doi: [10.3847/0004-637X/823/2/75](https://doi.org/10.3847/0004-637X/823/2/75)
- Schweizer, F., Seitzer, P., Kelson, D. D., Villanueva, E. V., & Walth, G. L. 2013, *The Astrophysical Journal*, 773, 148, doi: [10.1088/0004-637X/773/2/148](https://doi.org/10.1088/0004-637X/773/2/148)
- Shankar, F., Weinberg, D. H., & Miralda-Escudé, J. 2009, *The Astrophysical Journal*, 690, 20, doi: [10.1088/0004-637X/690/1/20](https://doi.org/10.1088/0004-637X/690/1/20)
- Shen, Y. 2021, *The Astrophysical Journal*, 921, 70, doi: [10.3847/1538-4357/ac1ce4](https://doi.org/10.3847/1538-4357/ac1ce4)
- Tombesi, F., Meléndez, M., Veilleux, S., et al. 2015, *Nature*, 519, 436, doi: [10.1038/nature14261](https://doi.org/10.1038/nature14261)
- Venturi, G., Nardini, E., Marconi, A., et al. 2018, *Astronomy and Astrophysics*, 619, A74, doi: [10.1051/0004-6361/201833668](https://doi.org/10.1051/0004-6361/201833668)
- Watkins, A. E., Mihos, J. C., Bershad, M., & Harding, P. 2018, *The Astrophysical Journal*, 858, L16, doi: [10.3847/2041-8213/aabba1](https://doi.org/10.3847/2041-8213/aabba1)
- Wei, P., Zou, H., Lin, L., et al. 2021, *Research in Astronomy and Astrophysics*, 21, 006, doi: [10.1088/1674-4527/21/1/6](https://doi.org/10.1088/1674-4527/21/1/6)
- Woo, J.-H., Bae, H.-J., Son, D., & Karouzos, M. 2016, *The Astrophysical Journal*, 817, 108, doi: [10.3847/0004-637X/817/2/108](https://doi.org/10.3847/0004-637X/817/2/108)
- Xu, X., & Wang, J. 2022, *The Astrophysical Journal*, 933, 110, doi: [10.3847/1538-4357/ac7222](https://doi.org/10.3847/1538-4357/ac7222)